Earth and Planetary Science Letters 311 (2011) 172–181

Contents lists available at SciVerse ScienceDirect

Earth and Planetary Science Letters

journal homepage: www.elsevier.com/locate/epsl

Seismic anisotropy of the uppermost mantle beneath the Rio Grande rift: Evidence from Kilbourne Hole peridotite xenoliths, New Mexico

Takako Satsukawa [a,b,*], Katsuyoshi Michibayashi [a,c], Elizabeth Y. Anthony [d], Robert J. Stern [e], Stephen S. Gao [f], Kelly H. Liu [f]

[a] Graduate School of Science and Technology, Shizuoka University, Ohya 836, Shizuoka 422-8529, Japan
[b] Géosciences Montpellier, Université Montpellier 2 and CNRS, Cc 060, Place E. Bataillon, 34095 Montpellier Cedex 5, France
[c] Institute of Geosciences, Shizuoka University, Ohya 836, Shizuoka 422-8529, Japan
[d] Department of Geological Sciences, University of Texas at El Paso, TX 79968, USA
[e] Department of Geosciences, University of Texas at Dallas, Richardson, TX 75080, USA
[f] Department of Geological Sciences and Engineering, Missouri University of Science and Technology, Rolla, MO 65409, USA

ARTICLE INFO

Article history:
Received 19 April 2011
Received in revised form 7 September 2011
Accepted 9 September 2011
Available online 4 October 2011

Editor: P. Shearer

Keywords:
peridotite xenolith
Kilbourne Hole maar
Rio Grande rift
mantle flow
crystallographic preferred orientation (CPO)
seismic anisotropy

ABSTRACT

Peridotite xenoliths from the Kilbourne Hole maar, New Mexico, consist of spinel lherzolite, harzburgite, and dunite. Because Kilbourne Hole erupted at approximately 10 ka, these xenoliths represent essentially current conditions beneath the Rio Grande rift. In this study, we present detailed petrofabric data and seismic properties obtained from peridotite xenoliths from Kilbourne Hole to illuminate the origin and significance of shear-wave splitting in the uppermost mantle beneath this active rift. Using phase relations and the temperature of equilibration, we infer that these xenoliths were derived from the uppermost mantle, from depths of 35–60 km. Their crystallographic preferred orientations indicate the preservation of olivine b-axis fiber fabrics with a strong concentration of [010] with girdles of [100] and [001]. We consider three geodynamic models for the source region of these xenoliths: horizontal extension, lateral shear, and upwelling. After calculating seismic properties using a volume fraction of olivine, orthopyroxene and clinopyroxene appropriate to each model, we conclude that these xenoliths are derived from a lateral shear zone (vertical foliation (XY plane) and horizontal lineation within the plane of the foliation (X-axis)). However, the degree of seismic anisotropy generated by peridotite xenoliths alone is limited, so that the existence of melt in thin cracks or dikes could be required to cause a significant increase; the orientation of such melt pockets parallel to the XY plane in either model would result in an increase in anisotropy. These results indicate that the shear-wave splitting observed in the Rio Grande rift is a reflection of the lithospheric fabric and the presence of melts as thin cracks or dikes.

1. Introduction

Continental rifting is a complex process involving deformation of the lithosphere, asthenospheric flow, and partial melting; each of these processes can result in seismically anisotropic structures. As such, the significance of shear-wave splitting, in particular whether it represents lithospheric fabric or asthenospheric flow, remains controversial (Gao et al., 2008). Recent passive seismological investigations, combined with CPO (crystallographic preferred orientation) studies of xenolith fabrics, have provided an inexpensive and fruitful avenue for addressing this question (e.g., Satsukawa et al., 2010). Measurements of shear-wave splitting using P-to-S converted phase (SKS, SKKS, and PKS) play a crucial role in imaging the orientation and degree of polarization of mantle fabrics and in constraining models for the formation of these fabrics (Liu, 2009; Savage, 1999; Silver, 1996). Numerous laboratory and field studies suggest that seismic anisotropy in the uppermost mantle results mainly from olivine CPO which tends to show a maximum seismic velocity parallel to the direction of plastic flow within the upper mantle (Nicolas and Christensen, 1987). This study is aimed at understanding mantle fabrics and their formation mechanisms beneath the Rio Grande rift by combining petrological and seismological measurements (Fig. 1).

The upwelling of asthenospheric mantle in rift zones provides an abundance of melts. Recent petrophysical studies of both natural (e.g., Le Roux et al., 2008) and experimentally generated (e.g., Holtzman et al., 2003) peridotites indicate that partial melting and refertilization processes may affect CPO. CPOs for peridotite xenoliths from the Kerguelen Islands, which are strongly affected by the Kerguelen plume, differ between harzburgites and dunites as a result of melt–rock interaction; these petrographic differences correspond with the distribution of CPO-induced S-wave anisotropy (Bascou et al., 2008).

* Corresponding author. Tel.: +81 54 238 4788; fax: +81 54 238 0491.
E-mail addresses: f5944004@ipc.shizuoka.ac.jp (T. Satsukawa), sekmich@ipc.shizuoka.ac.jp (K. Michibayashi), eanthony@geo.utep.edu (E.Y. Anthony), rjstern@utdallas.edu (R.J. Stern), sgao@mst.edu (S.S. Gao), liukh@mst.edu (K.H. Liu).

0012-821X/$ – see front matter © 2011 Elsevier B.V. All rights reserved.
doi:10.1016/j.epsl.2011.09.013

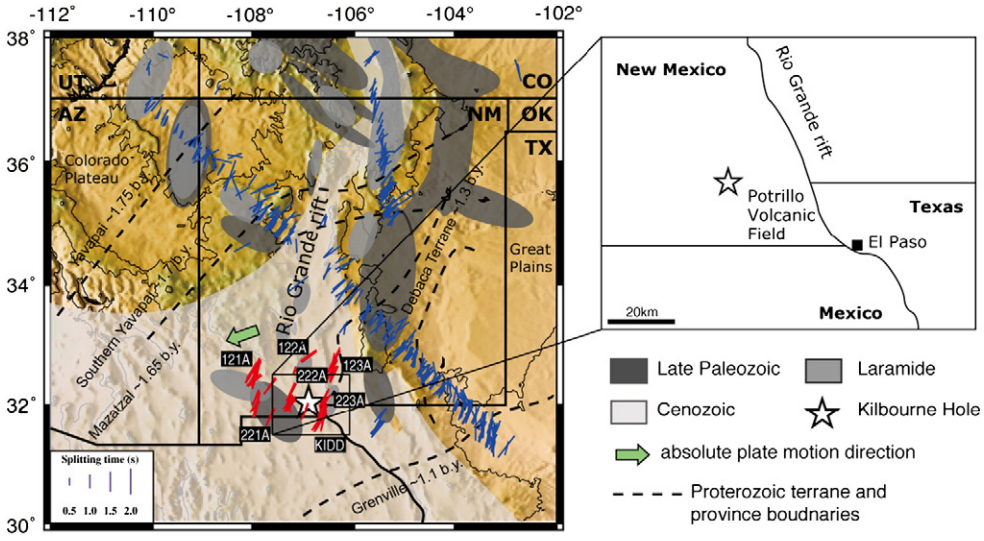

Fig. 1. Location of Kilbourne Hole maar in New Mexico, USA and shear-wave splitting parameters plotted above the XKS ray-piercing points at 100 km depth. The red bars are new splitting data in this study, and the blue bars are from the first uniform shear-wave splitting database (Liu, 2009). Note that in the original paper (Liu, 2009), the data were plotted above 200 km piercing points. To be consistent with the new results, we re-calculated the locations to 100 km depth. Absolute plate motion direction (green arrow) of North America calculated based on the HS3-NUVEL1A model (Gripp and Gordon, 2002). The orientation of the red bas represents the polarization direction of the fast wave, and the length of the bars is proportional to the splitting time which ranges from 0.45 s to 2.13 s, and the average splitting time is 1.2 ± 0.3 s. Uplift traces are modified after Wilson et al. (2003).

Previous studies have highlighted correlations between seismic properties and the modal composition of orthopyroxene and olivine, based on modeling (e.g., Mainprice, 1997), and analyses of natural sample of continental peridotite (e.g., Lee, 2003; Matsukage et al., 2005) and natural peridotite xenoliths (e.g., Pera et al., 2003; Soustelle and Tommasi, 2010). However, the effect of clinopyroxene on seismic properties is poorly understood, despite it having the third-highest modal abundance in peridotite.

Based on their observation of olivine CPO in Kilbourne Hole peridotite xenoliths from the Rio Grande rift, Bussod and Irving (1981) proposed that deformation was accompanied by syntectonic recrystallization in the presence of intercrystalline fluid. However, these samples were analyzed using a universal stage, and the seismic properties of the mantle beneath the Rio Grande rift were not considered. In this study, we present detailed petrofabric data for spinel peridotite xenoliths from Kilbourne Hole, New Mexico, determined using electron backscatter diffraction. Using these results, we illuminate the origin and significance of shear-wave splitting in the upper mantle beneath this active rift (Fig. 1).

2. Geological setting

The Kilbourne Hole maar exposes Quaternary basanites containing both crustal and mantle xenoliths (Hamblock et al., 2007). It is roughly elliptical in shape, almost 3 km in length, and from 100 to 125 m deep. Using ^{3}He surface exposure methods, the age of eruption has been constrained to 10–20 ka (Anthony and Poths, 1992; Williams, 1999); thus, the xenoliths represent essentially ambient conditions for the Rio Grande rift. Kilbourne Hole is a part of the Potrillo volcanic field (Anthony et al., 1992; Thompson et al., 2005), which consists of cinder cones, maars, and fissure flows of basanitic and alkalic basalt composition. The Potrillo volcanic field is one of the largest silica-undersaturated volcanic fields in the Rio Grande rift, and has been interpreted as representing the products of small-degree partial melting of a volatile-charged asthenosphere.

3. Seismic data

For the study, we use all available broadband seismic data recorded in the 2° by 2° area approximately centered at Kilbourne Hole. The data were recorded by 7 stations (Fig. 1) and were archived at the IRIS (Incorporated Research Institutions for Seismology) Data Management Center. Station KIDD is operated by the University of Texas at El Paso (UTEP) and is located near the UTEP campus, and the rest of the stations belong to the Transportable Array of the USArray. A robust shear-wave splitting parameter measuring and ranking procedure (Gao and Liu, 2009; Gao et al., 2010; Liu, 2009; Liu et al., 2008) developed based on the approach of Silver and Chan (1991) was applied to the broadband seismograms to obtain the polarization direction of the fast wave and the splitting time. A total of 84 pairs of well-defined splitting parameters were obtained (Fig. 1). The average fast direction is $22.0 \pm 11.7°$ from the North, which is sub-parallel to the strike of most regional tectonic features including the Rio Grande rift and Cenozoic faults in the area (Fig. 1). The average splitting time is 1.2 ± 0.3 s that is similar to the global average for continental areas (Silver, 1996). The waveforms, particle motion patterns and all the other related information for each of the measurements can be found at http://web.mst.edu/~sgao/XKS/KilHole/all/meas.html.

4. Mineral compositions, microstructures, and fabric analyses

We have studied six Kilbourne Hole peridotites, which span the modal ranges of lherzolite and harzburgite. In all samples the aluminous accessory phase was spinel, as is common for Cenozoic North American peridotite xenoliths (Wilshire et al., 1988). The silicate minerals have high Mg# ($Mg^{2+}/(Mg^{2+}+Fe^{2+})$), with Fo = 89–91 for olivine, En = 89–92 for orthopyroxene, and Mg# = 90–93 for clinopyroxene. Spinels exhibit a moderate depletion in Cr# ($Cr^{3+}/(Cr^{3+}+Al^{3+})$), ranging from 0.06 to 0.21 for lherzolite and from 0.22 to 0.51 for harzburgite. Based on texture, modal mineralogy, and chemical composition, the samples can be divided into three distinct groups. The first group comprises fine-grained (<2 mm) lherzolite with a tabular, equigranular texture (Fig. 2a). The second group consists of protogranular lherzolite (Fig. 2b); although its chemistry is still fertile, the fabric of these rocks is different from those of the first group. Although most previous studies of Kilbourne Hole xenoliths (e.g., Bussod and Irving, 1981) have considered only these two groups, we also identified a third group comprising porphyroclastic harzburgite (Fig. 2c). Xenoliths in this group are characterized by strong foliation and the whole-rock and mineral chemistries (Cr# in spinel) are consistent with melt depletion (Perkins and Anthony, 2011; Table 1). Using the thermometers of Brey and Köhler (1990), the equilibration temperatures (calculated at

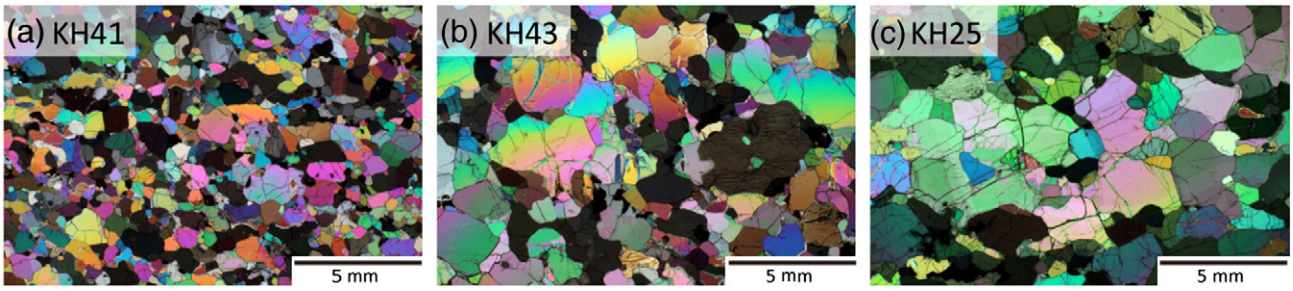

Fig. 2. Photomicrographs of peridotite xenoliths from Kilbourne Hole (scale bar is 5 mm). (a) KH41, fine grained lherzolite. (b) KH43, protogranular lherzolite. (c) KH25, porphyroclastic harzburgite.

2 GPa) of the three groups are also distinct: fine-grained lherzolite (KH41, KH29) has the lowest temperature (1009–1040 °C), protogranular to porphyroclastic lherzolite (KH43, KH54) has temperatures of 1049–1102 °C, and porphyroclastic olivine-rich peridotites (KH22, KH25) have the highest temperatures (1094–1152 °C; Table 1). Together with phase relations (Perkins and Anthony, 2011; Takahashi et al., 1993), these ranges imply that Kilbourne Hole xenoliths were derived from depths of 35–60 km, within the uppermost mantle. The difference in temperature in three textural types suggests that the subcontinental mantle beneath Kilbourne Hole is rheologically and chemically layered.

The peridotite xenoliths contain a foliation and a lineation defined by the alignment of spinel crystals; we have analyzed their microstructures using thin sections cut perpendicular to the foliation and parallel to the lineation (i.e., XZ sections). To examine the conditions of deformation in more detail, and to evaluate the effects of the seismic properties on rocks beneath the rift zone, we have focused on the CPOs of three common minerals: olivine, orthopyroxene, and clinopyroxene. These observations were obtained by electron backscatter diffraction (EBSD) using the SEM-EBSD facility at Géosciences Montpellier, France. The EBSD patterns were generated by the interaction of a vertical incident electron beam with a polished thin section, tilted at 70°, in a scanning electron microscope (JEOL JSM 5600). The diffraction pattern was projected onto a phosphor screen and recorded using a digital CCD camera. The resulting image was then processed and indexed in terms of crystal orientation using the CHANNEL5 software distributed by Oxford Instruments HKL. For each sample, we obtained CPO maps covering almost the entire thin section (usually 35 mm long and 20 mm wide), with sampling steps of 30 or 35 μm, depending on grain size; rates of indexation in the raw maps range from 50% to 80%. The measured CPOs are presented on equal-area, lower-hemisphere projections (Fig. 3). Most of the analyzed samples show a strong concentration in [010], with weak girdle of [100] and [001] in olivine. For orthopyroxene, although most of CPO patterns are weak, a (010)[001] pattern (shear direction is [001] and shear plane is (010)) occurs in two oriented samples (i.e. KH22 and 25). Clinopyroxene CPO data show nearly random fabrics, except for KH22, which show a weak (010)[001] slip.

To characterize CPOs, we determined the fabric strength (*J*-index) and distribution density (*pfJ*-index) of the principal crystallographic axes (for definitions of the *J*-index and *pfJ*-index, see Mainprice et al., 2000; Michibayashi and Mainprice, 2004). Table 1 lists the number of measured olivine grains, the *J*-index values calculated for each xenoliths, and the maximum density and *pfJ*-index value for each pole figure. The *J*-index is the volume-averaged integral of the squared orientation densities; it has a value of unity for a random CPO and is infinite for a single crystal. Most natural peridotites yield values between 2 and 20 (Ben Ismail and Mainprice, 1998), and those of the present study range from 2.81 to 9.65 (Table 1).

To maximize the average seismic anisotropy, the orientation data for each sample were adjusted to an external reference frame in which the maximum Vp is parallel to the reference direction X, and the minimum Vp is parallel to the Z-axis (see also Supplementary Fig. 1). By combining data from each of the six xenoliths, the average of the sample was then calculated, with the same weighting applied to each measurement, regardless of the number of measurements acquired from each xenolith (Supplementary Fig. 2a). Using this approach, olivine CPO data show b-axis fiber patterns characterized by a strong concentration in [010], with a weak girdle of [100] and [001]. For orthopyroxene, CPO data may indicate either or both (100)[001] and (010)[100] slip; the (100)[010] slip is the most readily activated, and thus the most common, slip system (Naze et al., 1987). In contrast, clinopyroxene CPO data suggest a nearly random fabric, with a weak concentration in (010) normal to the foliation (Supplementary Fig. 2a).

5. Rock seismic properties

Seismic properties were computed by averaging individual grain elastic-constant tensors as a function of the CPO and modal composition of a sample. This method enables the calculation of the three-dimensional

Table 1
Lithology, modal composition (%), number of measurements, *J*-index values (calculated after Mainprice et al., 2000), max density (MD), *pfJ* values, and temperature (Na/Opx-Cpx) for the six Kilbourne Hole peridotite xenoliths studied here.

Sample number	Lithology	Mode (%)			Grain size (mm)	CPO olivine								T (°C)	Ol Mg#	Sp Cr#
		Ol	Opx	Cpx		N	J	[100] axis		[010] axis		[001] axis				
								MD	pfJ	MD	pfJ	MD	pfJ			
KH41	Fine-grained lherzolite	56	26	18	0.52	734	2.81	4.46	1.63	1.90	1.11	3.97	1.37	1009	0.90	0.10
KH29	Fine-grained lherzolite	64	22	14	0.49	286	4.78	3.74	1.80	5.24	2.00	3.32	1.40	1040	0.89	0.07
KH43	Protogranular lherzolite	65	26	9	0.69	427	4.94	4.94	1.90	5.96	2.31	3.34	1.39	1049	0.89	0.10
KH54	Protogranular lherzolite	69	18	13	0.91	229	9.65	4.27	1.95	11.47	4.55	4.01	1.82	1102	0.89	0.11
KH22	Porphyroclastic harzburgite	77	17	5	1.20	319	6.11	4.39	1.97	8.01	2.86	3.70	1.46	1152	0.91	0.32
KH25	Porphyroclastic harzburgite	78	15	7	1.02	300	8.26	4.89	2.08	10.64	4.04	3.63	1.63	1094	0.91	0.22

Ol: olivine; Opx; orthopyroxene; Cpx: clinopyroxene; Sp: spinel; N: Number of measurements; J: *J*-index; MD: Maximum density; T: temperature, respectively.

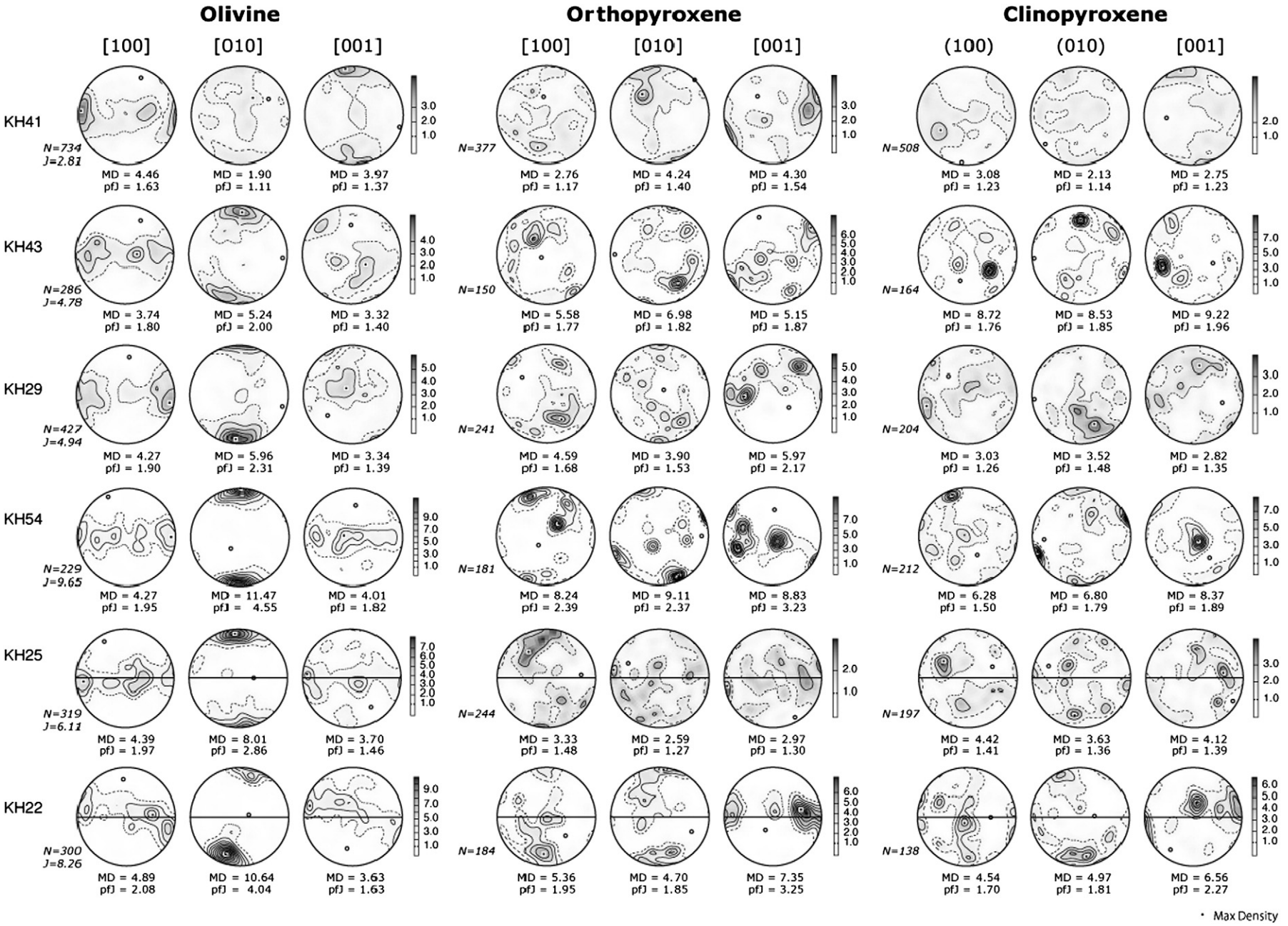

Fig. 3. Crystallographic preferred orientations (CPOs) of olivine, orthopyroxene and clinopyroxene. Lower hemisphere, equal-area stereographic projections, contours at one multiple of uniform distribution. N is number of measured grains.

distribution of seismic velocities in an anisotropic polycrystalline aggregate (Mainprice and Humbert, 1994). In the present calculations, we used Voigt–Reuss–Hill averaging of single-crystal elastic constants at ambient conditions (Abramson et al., 1997; Chai et al., 1997; Collins and Brown, 1998). Because the geothermobarometric analysis in this study yielded temperatures of 950–1200 °C and pressures of 1.3–1.8 GPa (Perkins and Anthony, 2011), we calculated the seismic properties assuming conditions of 1000 °C and 1.5 GPa (Supplementary Fig. 2b). This method has been described in detail previously (Pera et al., 2003; Tasaka et al., 2008).

On average, olivine CPOs have P-wave propagation that is fastest parallel to the highest density of [100], and is slowest parallel to the highest density of [010]; polarization anisotropies are highest in directions approximately normal to the highest density of [010]. The orientation of the polarization plane of the fastest S-wave (Vs_1) indicates the orientation of the great circle containing the [100] maximum. The Vp of olivine range from 7.58 to 8.24 km/s; their anisotropy is 8.4% and AVs_{max} is 6.88%. For orthopyroxene CPOs, the average anisotropies are small: Vp range between 7.72 and 7.78 km/s, their anisotropy is 0.8%, and AVs_{max} is 1.72%. Although clinopyroxene has weaker CPOs and smaller measured values than orthopyroxene, its seismic anisotropy is larger: Vp range between 8.28 and 8.61 km/s, their anisotropy is 3.9%, and AVs_{max} is 2.22%.

To assess the effect of grain size, we also calculated seismic properties from grid data obtained from CPO maps (Supplementary Fig. 2c). The distributions of seismic properties calculated in this way are very similar to those listed above based on a single measurement per grain (Supplementary Fig. 2b), although individual velocity and anisotropy values calculated from grid data shown an increase compared to that from single measurement data per grain (e.g., for olivine, Vp range between 7.45 and 8.42 km/s, their anisotropy is 12.3%, and AVs_{max} is 9.17%). In this paper, we prefer the seismic properties based on the grid data (Supplementary Fig. 2c) to those based on a single measurement per grain (Supplementary Fig. 2b) for the following interpretations, which contains the effect of grain size, and thus it will provide more realistic seismic properties.

6. Variation in seismic properties as a function of modal composition

Based on the modal composition of peridotites (four lherzolites and two harzburgites), we recalculated the seismic properties for mean compositions of dunite (Ol_{100}), harzburgite ($Ol_{78}Opx_{16}Cpx_6$), and lherzolite ($Ol_{64}Opx_{23}Cpx_{13}$; Fig. 4). Using this approach, P-wave propagation is fastest parallel to the highest density of [100] and is slowest parallel to the highest density of [010], and polarization anisotropies are highest at directions approximately normal to the highest density of [010]. Vp/Vs_1 and Vp/Vs_2 ratios are highest for propagation directions that are normal and parallel, respectively, to the highest density of [100] of olivine. Although these anisotropy patterns do not change significantly as olivine volume fraction decreases, P- and S-wave velocities and anisotropies decrease. Because olivine is the primary mineral in peridotites, it is likely that peridotite anisotropy is defined mainly by the characteristics of olivine.

We have calculated variations in seismic properties as a function of modal composition for the structural planes of XY for horizontal shear, XZ for lateral shear, and YZ for vertical shear (Fig. 5); in these figures, gray shaded squares represent ranges in the modal compositions of peridotite xenoliths from this study. To estimate the effect of modal composition on seismic properties, we varied the mineral composition from 100% olivine to 50% olivine + 50% pyroxene, by the alternating stepwise addition of 10% orthopyroxene or clinopyroxene. In Fig. 5, we have extrapolated variations in Vp anisotropy, the maximum Vs anisotropy, Vp, the anisotropy of Vs, the average of Vp, the deviation of Vp, and Vp/Vs with respect to the olivine volume fraction, assuming propagation direction of seismic wave is vertical. As a result, the effect of the second most abundant phase on seismic properties is highly dependent on structural orientation. Vp anisotropy decreases as the volume fraction of olivine decreases (Fig. 5a), whereas average Vp, unlike other factors, increases with the addition of clinopyroxene (i.e., decreasing olivine abundance; Fig. 5b, d). Vp/Vs does not differ significantly as a function of modal olivine abundance.

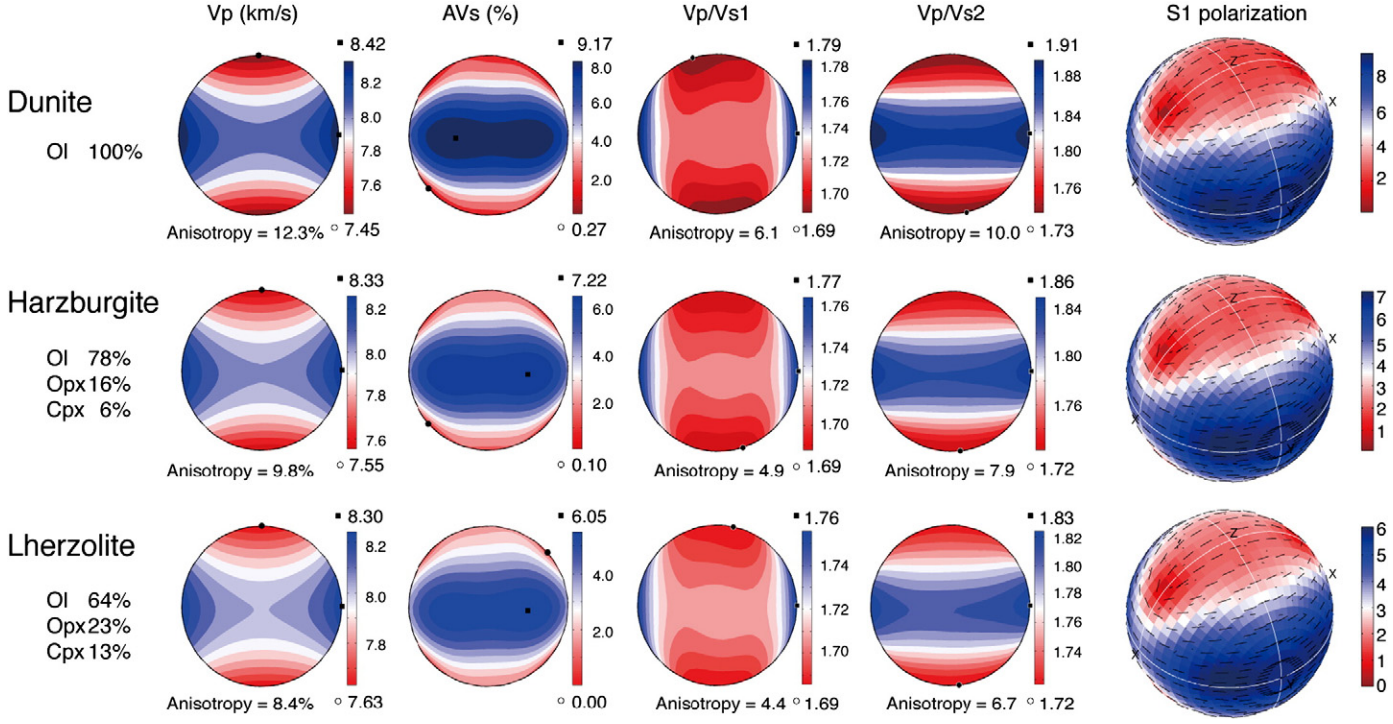

Fig. 4. Seismic properties of the average dunite, harzburgite, and lherzolite (from Supplementary Fig. 2a) at a temperature of 1000 °C and a pressure of 1.5 GPa. From left to right: P-wave velocity, S-wave anisotropy, Vp/Vs_1, Vp/Vs_2, and the polarization of the fast shear wave S_1.

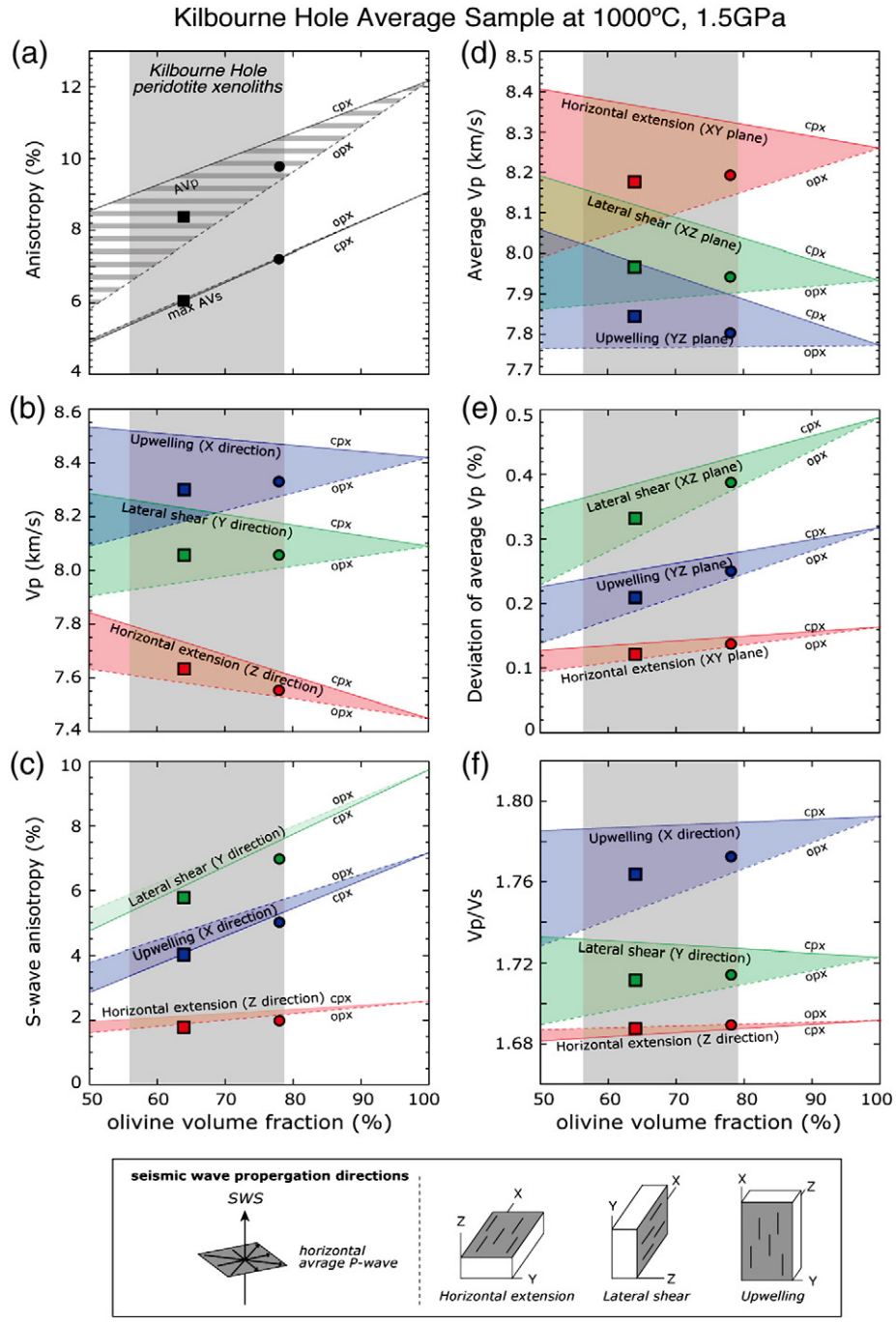

Fig. 5. Variations in (a) Vp anisotropy and the maximum Vs anisotropy, (b) Vp, (c) S-wave anisotropy, (d) Average Vp, (e) Deviation of average Vp and (f) Vp/Vs as a function of mantle composition at a temperature of 1000 °C and pressure of 1.5 GPa. Solid lines represent compositions ranging from 50% olivine + 50% clinopyroxene to 100% olivine; broken lines represent compositions ranging from 50% olivine + 50% orthopyroxene to 100% olivine. Contours are shown for three geodynamic models: red for horizontal extension, green for lateral shear, and blue for upwelling. Within the box, the shaded area represents the plane of the foliation, and lines indicate lineation. Symbols relate to the mean composition of the peridotites: squares for lherzolite and circles for harzburgite.

7. Discussion: Seismic anisotropies beneath the Rio Grande rift

Because the peridotite xenoliths in this study erupted recently (10 ka), they provide a snapshot of the "present" mantle composition beneath the region in central New Mexico known as the Rio Grande rift. Isotopic studies suggest that all lithosphere that formed or was reworked during past tectonics events are preserved (Anthony, 2005). Kilbourne Hole peridotite xenoliths come from a depth range of 35–60 km, the lowest-temperature samples potentially represent lithospheric mantle, whereas those from higher temperatures may represent the asthenosphere. CPO patterns are characterized by a strong concentration of [010], which show normal distribution compared to another peridotite xenoliths from a continental margin setting in Knippa, Texas (Satsukawa et al., 2010). In addition, some seismic properties are different between the two sets of xenoliths, such as polarization anisotropies, which have maximums approximately parallel to the foliation for Kilbourne Hole peridotite xenoliths, but normal to foliation for Knippa peridotite xenoliths (Satsukawa et al., 2010).

The geometry and strength of seismic anisotropies are generally estimated using measurements of shear-wave splitting, which can

place constraints on both the delay time and polarization direction of fast shear-wave propagation. Shear-wave splitting results indicate a delay time of 0.45–2.13 s with the average splitting time 1.2 ± 0.3 s within the Rio Grande rift (Fig. 1).

Continental rifting is a complex process involving deformation of the lithosphere, asthenospheric flow, and partial melting. Because each of these processes may result in seismically anisotropic structures, it is difficult to discriminate between the effects of rock anisotropy, recent mantle flow, and aligned cracks (Gao et al., 1997). In addition, Vauchez et al. (2000) showed that an anisotropy due to preferentially oriented anisometric melt pockets may add to the asthenospheric CPO-induced anisotropy beneath the active part of a rift. In this paper, we present seismic properties obtained from peridotite xenoliths from Kilbourne Hole, which we use to discuss rock seismic properties, as well as other mineral phases.

Lherzolite xenoliths generally contain orthopyroxene in higher abundances than clinopyroxene, which is a result of the selective removal of clinopyroxene from primary mantle lherzolite by partial melting. In spite of its small volume fraction, clinopyroxene has a significant effect on seismic properties (Fig. 5). It is also interesting to note that in the case of harzburgite ($Ol_{78}Opx_{16}Cpx_6$) and lherzolite ($Ol_{64}Opx_{23}Cpx_{13}$) mineral compositions, S-wave anisotropy is lower than results calculated from either orthopyroxene or clinopyroxene alone (Fig. 5c). This may reflect an offset of the S-wave anisotropy (AVs) caused by interactions between orthopyroxene and clinopyroxene (Supplementary Fig. 2b, c).

The magnitude of the delay time depends on the strength of the anisotropy and the thickness of the anisotropic layer. To explain the variability in splitting times near Kilbourne Hole, the thickness (T) of an anisotropic layer can be described by $T = (100\ dt{<}Vs{>})/AVs$ (e.g., Pera et al., 2003). Although the original orientation of the Kilbourne Hole xenoliths was lost during transport to the surface, we know from their mineral compositions that they were derived from the uppermost lithospheric mantle (Perkins and Anthony, 2011). We have calculated the thickness of the anisotropic layer with our averaged sample (Supplementary Fig. 2) using the average splitting time (1.2 s) for three different structural orientations. This allowed us to assess the degree to which the CPO data are consistent with models in which horizontal extension, lateral shear, or upwelling are invoked to explain the observed delay time (Fig. 6). Using this approach, we obtain anisotropic layer thicknesses (for models of lateral shear, upwelling, and horizontal extension, respectively) of 70–110, 100–180 and 260–350 km for a delay time of 1.2 s (Fig. 6).

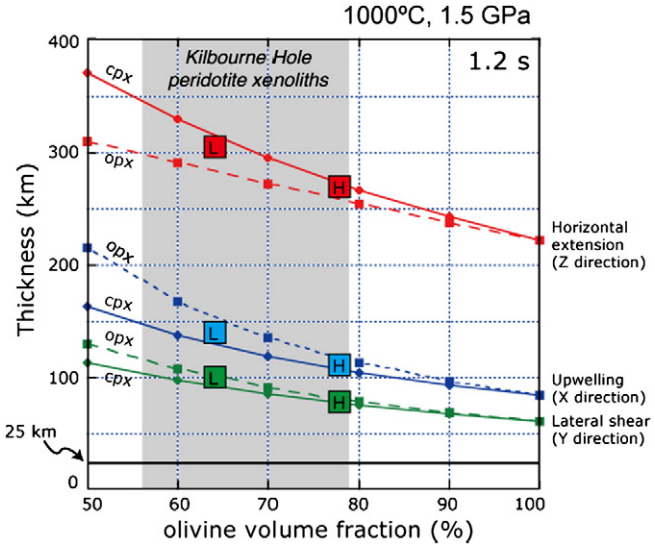

Fig. 6. Relationship between olivine volume fraction and required thickness of the anisotropic layer in Kilbourne Hole, as indicated by peridotite xenoliths. Delay time is 1.2 s. H and L are the harzburgite and lherzolite shown in Fig. 4, respectively.

Of these results, only the lateral shear and upwelling models yield thicknesses consistent with geothermobarometric evidence that the peridotite xenoliths came from a depth of 35–60 km. Because the study region is an active rift zone, these two models are also suitable from a geological perspective. For example, Vauchez et al. (2000) proposed that anisotropies measured in the Rio Grande rift were caused by a transtensional deformation of the lithospheric mantle during rifting, as indicated by the consistent obliqueness of the polarization direction of the fast shear wave to the rift trend. However, it should be noted that when a delay time of 1.2 s is used, our calculated thicknesses of the anisotropic layer are still greater than those indicated by geothermobarometric evidence (25 km; Fig. 6).

Other factors, such as the alignment of melt lenses in the low-velocity zone, or cracks infilled by fluid, may provide a more likely explanation for the observed seismic anisotropy, and seismological studies do favor the existence of melts beneath the Rio Grande rift. A wide zone of low velocity situated beneath the Rio Grande rift, at a depth of 65 to 125 km, is clearly visible in LA RISTRA data obtained using both surface wave inversions (West et al., 2004) and tomography (Gao et al., 2004). Velocities from depths of 55 to 90 km beneath the rift axis are 10% slower than those beneath the Great Plains, which is consistent with the presence of small amounts of partial melt (West et al., 2004). Thus, SKS splitting measurements in the Rio Grande rift could also be caused by magma-filled cracks (e.g., Gao et al., 1997).

Seismological studies using travel-time tomography reveal the existence of a low-velocity zone within the mantle wedge (e.g., Nakajima and Hasegawa, 2004). The Vp/Vs ratio provides constraints on mantle composition, in particular for low-velocity zones in the mantle wedges (e.g., Nakajima et al., 2001). Several models have been proposed to explain spatial variation of Vp/Vs ratios, including the presence of fluids or melts for high ratios of Vp/Vs (Takei, 2002), or changes in mineralogical composition (e.g., orthopyroxene enrichment) for low ratios of Vp/Vs (Wagner et al., 2006).

Enrichment in orthopyroxene is widely reported for peridotite xenoliths (Griffin et al., 2008; Soustelle et al., 2010); Vp/Vs ratios calculated from spinel peridotite xenoliths from Avacha volcano in Kamchatka, vary from 1.72 to 1.75, and decrease with increasing orthopyroxene content (Soustelle and Tommasi, 2010). In addition, Vp/Vs ratios from different tectonic settings show a better correlation with the abundance of orthopyroxene than that of olivine (Afonso et al., 2010). In our model, Vp/Vs ratios vary from 1.68 to 1.78 (Fig. 5f) and decrease with increasing of orthopyroxene composition, but the ratios are almost insensitive to the degree of clinopyroxene enrichment in all of our models (upwelling, lateral shear, and horizontal extension). As a result, the variability in Vp/Vs ratios is minimal for our natural peridotite compositions (harzburgite: $Ol_{78}Opx_{16}Cpx_6$; lherzolite: $Ol_{64}Opx_{23}Cpx_{13}$). Thus, we predict that for most of the upper mantle, compositional variations are unlikely to alter Vp/Vs ratios to a detectable degree in terms of current seismological methods.

As discussed above, the use of models that consider only mineral CPOs makes it difficult to produce realistic thicknesses for the anisotropic layer, or meaningful Vp/Vs ratios from rock seismic anisotropies. Another possibility is to use the preferential orientation of melt-lenses as an additional phase in the models. By applying the approach developed by Mainprice (1997), Vauchez et al. (2000) used simulations to show that if melt is contained in isometric or weakly anisometric pockets, an increase in melt fraction alone does not significantly increase the anisotropy of an aggregate. In contrast, if even small amounts of melt (e.g., 4%) collect in thin lenses parallel to the foliation, they can double the anisotropy produced by the mineral CPO, indicating that melt lenses may contribute significantly to seismic anisotropy within the rift itself. Nakajima et al. (2005) evoked the existence of melt-filled pores, combined with a specific effective aspect ratio and volume fraction for the pores, to explain the observed low-velocity anomalies in NE Japan, which cannot be

explained by the thermal effect alone. For a depth of 40 km, this approach results in 1–2 vol.% melts, present as thin cracks or dikes with aspect ratios of 0.02–0.04, whereas a depth of 65 km yields 0.04–0.05 vol.% melt with an aspect ratio of ~0.001.

We can compare the shear wave splitting of dt = 1.2 (±0.3) s for the Rio Grande rift to another well-studied rift zone in Ethiopia (where the splitting is greater and varies from 1.7 to 2.5 s; Kendall et al., 2005). In addition, APM (absolute plate motion) direction is nearly parallel to the rift for the Rio Grande, whereas in Ethiopia, it is almost perpendicular. Considering these observations and that degree of melting is rather small in the Rio Grande rift, the model that has the maximum CPO related shear wave splitting with Y vertical (i.e., the lateral shear model) is more realistic for the Rio Grande, even if a small amount of melt is present. The orientation of APM direction with respect to the rift axis is also more compatible with lateral shear.

In this study, we propose a schematic model for the structure of the uppermost mantle beneath the Rio Grande rift, based on evidence from peridotite xenoliths from the Kilbourne Hole maar, derived from depths of 35–60 km (Fig. 7). Models of lateral shear is likely to contribute to the thickness of the anisotropic layer (Fig. 6). Moreover, the vertically planar structure of these models is in good agreement with the observed high concentrations of [010] in olivine, parallel to the Z direction. In the lateral shear model (considered relative to the XZ plane), the polarization direction of Vs_1 (the fastest S-wave) is in the XY plane (Fig. 4). Because the shear-wave splitting direction is parallel to the rift axis, we assume that the Z direction is normal to the rift axis (Fig. 7), which is most reasonable from a geological perspective.

The degree of S-wave anisotropy generated by peridotite xenoliths alone is limited; it is 4.81 to 8.82%, however it requires approximately 13 to 17% to produce the realistic thickness (25 km). Therefore the existence of melt in thin cracks or dikes could be required to cause a significant increase. It is well established that melt reduces shear-wave velocity; consequently, seismic anisotropy is sensitive to the orientation of melt pockets. It is likely that melt pockets could be ideally oriented parallel to the XY plane in either model, so that the velocity of S2 may be lower, resulting in an increase in anisotropy (Fig. 7). In contrast, the orientation of such melt pockets parallel to the YZ plane would reduce the velocity of S1 but would not affect S2 velocities (Fig. 7), resulting in lower anisotropies. We can estimate the melt fractions and shape of melts pocket to produce high S-wave anisotropy (13 to 17%) if we apply the result of simulation by Vauchez et al. (2000) to this study. In case of 20 (shape ratio; 20:20:1), melt fraction is 1.5 to 2.5%. On the other hand, it requires 6 to 9% of melt fraction for the case of 5 (5:5:1).

8. Conclusions

Continental rifting is a complex process involving deformation of the lithosphere, asthenospheric flow, and partial melting. Because each of these processes may result in seismically anisotropic structures, it is difficult to discriminate between the effects of rock anisotropy, recent mantle flow, and aligned cracks. In this paper, we present detailed petrofabric data and seismic properties obtained from peridotite xenoliths from Kilbourne Hole to illuminate the origin and significance of shear-wave splitting in the uppermost mantle beneath this active rift. Peridotite xenoliths from the Kilbourne Hole maar consist of spinel lherzolite, harzburgite, and dunite, which were derived from the uppermost mantle, from depths of 35 to 60 km. Since Kilbourne Hole erupted at approximately 10 ka, these xenoliths represent essentially current conditions beneath the Rio Grande rift. Their crystallographic preferred orientations indicate the preservation of olivine b-axis fiber fabrics with a strong concentration of [010] with girdles of [100] and [001].

We consider three geodynamic models for the source region of these xenoliths: horizontal extension, lateral shear, and upwelling, using a volume fraction of orthopyroxene and clinopyroxene appropriate to each model. Although lherzolite xenoliths generally contain

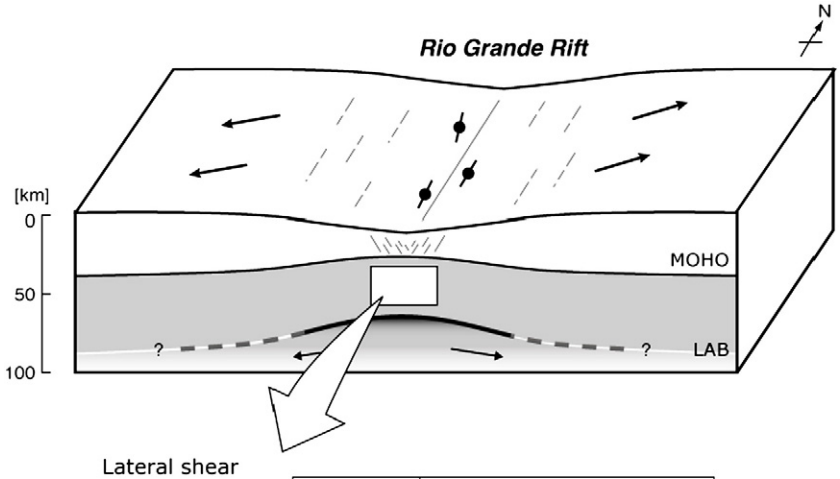

shape and orientation of an ideal melt	Case 1. // XY	Case 2. // XZ
S1	-	lower
S2	lower	-
Anisotropy	higher	lower

Fig. 7. Schematic summary of results showing the possible type of model (lateral shear zone), and the shape and orientation of an ideal melts beneath the Rio Grande rift.

orthopyroxene in higher abundances than clinopyroxene, clinopyroxene has a significant effect on seismic properties, in spite of its small volume fraction. After calculating seismic properties and consideration of absolute plate motion direction, we conclude that these xenoliths are derived from a lateral shear zone (vertical foliation (XY plane) and horizontal lineation within the plane of the foliation (X-axis)). However, the degree of seismic anisotropy generated by peridotite xenoliths alone is limited, so that the existence of melt in thin cracks or dikes could be required to cause a significant increase. If melt pockets are oriented parallel to the XY plane in either model, the velocity of S2 may be lower, resulting in an increase in anisotropy. In contrast, the orientation of such melt pockets parallel to the YZ plane would reduce the velocity of S1 but would not affect S2 velocities, resulting in lower anisotropies.

Overall, the peridotite xenoliths demonstrate the possible presence of an anisotropic layer within the uppermost mantle lithosphere, which could be related to 'frozen' deformation. We have calculated the maximized seismic properties of peridotite xenoliths in order to determine their contribution to seismic observations of the active region of the Rio Grande rift. In summary, the seismic properties determined for the mantle beneath the rift suggest that the region has a complex tectonic pattern, with probable lateral shear, in addition to the presence of melt as thin cracks or dikes.

Acknowledgements

Drawings of CPO and calculations of the *J*-index and seismic anisotropy were performed using the interactive programs developed by D. Mainprice of Université Montpelier II, France. We thank the IRIS DMS for providing the seismic waveform data used in the study and F. Barou of Université Montpelier II for help with EBSD analysis. Thoughtful reviews by anonymous referees. This work was supported by a Grant-in-Aid for Scientific Research (223708) as part of a JSPS Research Fellowship for Young Scientists (to TS), and research grants from JSPS (22244062, to KM), the Norman Hackerman Advanced Research Program 003661-0003-2006 (to EYA and RJS) and the US National Science Foundation awards EAR-0739015 and EAR-0952064 (to KHL and SSG).

Appendix A. Supplementary data

Supplementary data to this article can be found online at doi:10.1016/j.epsl.2011.09.013.

References

Abramson, E.H., Brown, J.M., Slutsky, L.J., Zang, J.J., 1997. The elastic constants of San Carlos olivine to 17 GPa. J. Geophys. Res. 102, 12253–12263.
Afonso, J.C., Ranalli, G., Fernandez, M., Griffin, W.L., O'Reilly, S.Y., Faul, U., 2010. On the Vp/Vs-Mg# correlation in mantle peridotites: implication for the identification of thermal and compositional anomalies in the upper mantle. Earth Planet. Sci. Lett. 289, 606–618.
Anthony, E.Y., 2005. Source regions of granites and their links to tectonic environment: examples from the western United States. Lithos (Ilmari Haapala Retirement Special Volume) 80, 61–74.
Anthony, E.Y., Poths, J., 1992. 3He surface exposure dating and its implications for magma evolution in the Potrillo volcanic field, Rio Grande Rift, New Mexico, USA. Geochim. Cosmochim. Acta 56, 4105–4108.
Anthony, E.Y., Hoffer, J.M., Wagner, W.K., Chen, W., 1992. Compositional diversity in late Cenozoic mafic lavas in the Rio Grande rift and Basin and Range province, southern New Mexico. Geol. Soc. Am. Bull. 104, 973–979.
Bascou, J., Deipech, G., Vauchez, A., Moine, B.N., Cottin, J.Y., Barruol, G., 2008. An integrated study of microstructural, geochemical, and seismic properties of the lithospheric mantle above the Kerguelen plume (Indian Ocean). Geochem. Geophys. Geosyst. 9, Q04036. doi:10.1029/2007GC001879.
Ben Ismail, W., Mainprice, D., 1998. An olivine fabric database: an overview of upper mantle fabrics and seismic anisotropy. Tectonophysics 296, 145–157.
Brey, G.P., Köhler, T., 1990. Geothermobarometry in four-phase lherzolites II. New thermobarometers, and practical assessment of existing thermobarometers. J. Petrol. 31, 1353–1378.
Bussod, G.Y.A., Irving, A.J., 1981. Thermal and rheologic history of the upper mantle beneath the Southern Rio Grande Rift: evidence from Kilbourne Hole xenoliths. Conference on the Processes of Planetary Rifting. Lunar and Planetary Institute, pp. 145–148.
Chai, M., Brown, J.M., Slutsky, L.J., Zang, J., 1997. The elastic constants of an aluminous orthopyroxene to 12.5 GPa. J. Geophys. Res. 102, 14779–14785.
Collins, M.D., Brown, J.M., 1998. Elasticity of an upper mantle clinopyroxene. Phys. Chem. Miner. 26, 7–13.
Gao, S.S., Liu, K.H., 2009. Significant seismic anisotropy beneath the southern Lhasa Terrane, Tibetan Plateau. Geochem. Geophys. Geosyst. 10, Q02008. doi:10.1029/2008GC002227.
Gao, S., Davis, P.M., Liu, H., Slack, P.D., Rigor, A.W., Zorin, Y.A., Mordvinova, V.V., Kozhevnikov, V.M., Logatchev, N.A., 1997. SKS splitting beneath continental rift zones. J. Geophys. Res. 102 (B10), 22781–22797.
Gao, W., Grand, S.P., Baldridge, W.S., Wilson, D., West, M., Ni, J.F., Aster, R., 2004. Upper mantle convection beneath the central Rio Grande rift imaged by P and S wave tomography. J. Geophys. Res. 109, B03305. doi:10.1029/2003JB002743.
Gao, S.S., Liu, K.H., Stern, R.J., Keller, G.R., Hogan, J.P., Pulliam, J., Anthony, E.Y., 2008. Characteristics of mantle fabrics beneath the south-central United States: constraints from shear-wave splitting measurements. Geosphere 4 (2), 411–417.
Gao, S.S., Liu, K.H., Abdelsalam, M.G., 2010. Seismic anisotropy beneath the Afar Depression and adjacent areas: implications for mantle flow. J. Geophys. Res. 115, B12330. doi:10.1029/2009JB007141.
Griffin et al., 2008, J. PetrolGrif!n, W.L., O'Reilly, S.Y., Afonso, J.C., Begg, G., 2008. The composition and evolution of lithosphericmantle: a re-evaluation and its tectonic implications. J. Petrol.. doi:10.1093/petrology/egn033.
Gripp, A.E., Gordon, R.G., 2002. Young tracks of hotspots and current plate velocities. Geophys. J. Int. 150, 321–361.
Hamblock, J.M., Andronicos, C.L., Miller, K.C., Barnes, C.G., Ren, M.-H., Averill, M.G., Anthony, E.Y., 2007. A composite geologic and seismic profile beneath the southern Rio Grande rift, New Mexico, based on xenoliths mineralogy, temperature, and pressure. Tectonophys 442, 14–48.
Holtzman, B.K., Kohlstedt, D.L., Zimmerman, M.E., Heidelbach, F., Hiraga, T., Hustoft, J., 2003. Melt segregation and strain partitioning: implications for seismic anisotropy and mantle flow. Science 301, 1227–1230. doi:10.1126/science.1087132.
Kendall, J.-M., Stuart, G.W., Ebinger, C.J., Bastow, I.D., Keir, D., 2005. Magma-assisted rifting in Ethiopia. Nature 433, 146–148.
Le Roux, V., Tommasi, A., Vauchez, A., 2008. Feedback between melt percolation and deformation in an exhumed lithosphere-asthenosphere boundary. Earth Planet. Sci. Lett. 274, 401–413.
Lee, C.-T.A., 2003. Compositional variation of density and seismic velocities in natural peridotites at STP conditions: implications for seismic imaging of compositional heterogeneites in the upper mantle. J. Geophys. Res. 108. doi:10.1029/2003JB002413.
Liu, K.H., 2009. NA-SWS-1.1: a uniform database of teleseismic shear wave splitting measurements for North America. Geochem. Geophys. Geosyst. 10, Q05011. doi:10.1029/2009GC002440.
Liu, K.H., Gao, S.S., Gao, Y., Wu, J., 2008. Shear wave splitting and mantle flow associated with the deflected Pacific slab beneath northeast Asia. J. Geophys. Res. 113, B01305. doi:10.1029/2007JB005178.
Mainprice, D., 1997. Modelling anisotropic seismic properties of partially molten rocks found at mid-ocean ridges. Tectonophys 279, 161–179.
Mainprice, D., Humbert, M., 1994. Methods of calculating petrophysical properties from lattice preferred orientation data. Surv. Geophys. 15, 575–592.
Mainprice, D., Barruol, G., Ben Ismail, W., 2000. The anisotropy of the Earth's mantle: from single crystal to polycrystal. In: Karato, S., et al. (Ed.), Mineral Physics and Seismic Tomography: From Atomic to Global. : Geophys. Monogr. Ser., vol. 117. AGU, Washington, D. C, pp. 237–264.
Matsukage, K.M., Nishihara, Y., Karato, S.I., 2005. Seismological signature of chemical differentiation of Earth's upper mantle. J. Geophys. Res. 110, B12305. doi:10.1029/2004JB003504.
Michibayashi, K., Mainprice, D., 2004. The role of pre-existing mechanical anisotropy on shear zone development within oceanic mantle lithosphere: and example from the Oman ophiolites. J. Petrol. 45 (2), 405–414. doi:10.1093/petrology/egg099.
Nakajima, J., Hasegawa, A., 2004. Shear-wave polarization anisotropy and subduction-induced flow in the mantle wedge of northeastern Japan. Earth Planet. Sci. Lett. 225, 365–377.
Nakajima, J., Matsuzawa, T., Hasegawa, A., Zhao, D., 2001. Threedimensional structure of Vp, Vs, and Vp/Vs beneath the northeastern Japan arc: implications for arc magmatism and fluids. J. Geophys. Res. 106, 21843–21857.
Nakajima, J., Takei, Y., Hasegawa, A., 2005. Quantitative analysis of the inclined low-velocity zone in the mantle wedge of northeastern Japan: a systematic change of melt-filled pore shapes with depth and its implications for melt migration. Earth Planet. Sci. Lett. 234, 59–70.
Naze, L., Doukhan, N., Doukhan, J.C., Latrous, K., 1987. TEM study of lattice defects in naturally and experimentally deformed orthopyroxenes. Bull. Miner. 110, 497–512.
Nicolas, A., Christensen, N.I., 1987. Formation of anisotropy in upper mantle peridotites: a review. In: Fuchs, K., Froidevaux, C. (Eds.), Composition, Structure and Dynamics of the Lithosphere-Asthenosphere System. : Geodyn. Ser., vol. 16. AGU, Washington, D. C, pp. 111–123.
Pera, E., Mainprice, D., Burlini, L., 2003. Anisotropic seismic properties of the upper mantle beneath the Torre Alfina area (northern Apennines, central Italy). Tectonophys 370, 11–30.
Perkins, D., Anthony, E.Y., 2011. The evolution of spinel lherzolite xenoliths and the nature of the mantle at Kilbourne Hole, New Mexico. Contrib. Miner. Petrol. doi:10.1007/s0410-011-0644-1
Satsukawa, T., Michibayashi, K., Raye, U., Anthony, E.Y., Pulliam, J., Stern, R., 2010. Uppermost mantle anisotropy beneath the southern Laurentian margin: evidence from Knippa peridotite xenoliths, Texas. Geophys. Res. Lett. 37, L20312. doi:10.1029/2010GL044538.
Savage, M.K., 1999. Seismic anisotropy and mantle deformation: what have we learned from shear wave splitting? Rev. Geophys. 37, 65–106.
Silver, P.G., 1996. Seismic anisotropy beneath the continents: probing the depths of geology. Annu. Rev. Earth. Planet. Sci. 24, 385–432.

Silver, P.G., Chan, W.W., 1991. Shear wave splitting and subcontinental mantle deformation. J. Geophys. Res. 96, 16429–16454.

Soustelle, V., Tommasi, A., 2010. Seismic properties of the supra-subduction mantle: constraints from peridotite xenoliths from the Avacha volcano, southern Kamchatka. Geophys. Res. Lett. 37, L13307. doi:10.1029/2010GL043450.

Soustelle, V., Tommasi, A., Demouchy, S., Ionov, D.A., 2010. Deformation and fluid–rock interaction in the supra-subduction mantle: microstructures and water contents in peridotite xenoliths from the Avacha Volcano, Kamchatka. J. Petrol. 51 (1&2), 363–394. doi:10.1093/petrology/egp085.

Takahashi, E., Shimazaki, T., Tsuzaki, Y., Yoshida, H., 1993. Melting study of a peridotite KLB-1 to 6.5 GPa, and the origin of basaltic magmas. Phil. Trans. R. Soc. Lond. A. 342, 105–120.

Takei, Y., 2002. Effect of pore geometry on VP/VS: from equilibrium geometry to crack. J. Geophys. Res. 107 (B2), 2043. doi:10.1029/2001JB000522.

Tasaka, M., Michibayashi, M., Mainprice, D., 2008. B-type olivine fabrics developed in the fore-arc side of the mantle wedge along a subducting slab. Earth Planet. Sci. Lett. 272, 747–757.

Thompson, R.N., Ottley, C.J., Smith, P.M., Pearson, D.G., Dickin, A.P., Morrison, M.A., Leat, P.T., Gibson, S.A., 2005. Source of the quaternary alkalic basalts, pictrites and basanites of the Potrillo Volcanic Field, New Mexico, USA: lithosphere or convecting mantle? J. Petrol. 46, 1603–1643.

Vauchez, A., Tommasi, A., Barruol, G., Manumus, J., 2000. Uppermost mantle deformation and seismic anisotropy in continental rifts. Phys. Chem. Earth (A) 25 (2), 111–117.

Wagner, L.S., Beck, S., Zandt, G., Ducea, M.N., 2006. Depleted lithosphere, cold, trapped asthenosphere, and frozen melt puddles above the flat slab in central Chile and Argentina. Earth Planet. Sci. Lett. 245, 289–301. doi:10.1016/j.epsl.2006.02.014.

West, M., Ni, J., Baldridge, W.S., Wilson, D., Aster, R., Gao, W., Grand, S., 2004. Crust and upper mantle shear wave structure of the southwest United States: implications for rifting and support for high elevation. J. Geophys. Res. 109, B03309. doi:10.1029/2003JB002575.

Williams, W. J. W., 1999. Evolution of Quaternary intra plate mafic lavas from the Potrillo volcanic field, USA, and the San Quintin volcanic field, Mexico. Univ. Texas at El Paso. Unpub PhD dissertation, 186p.

Wilshire, H.G., Meyer, C.E., Nakata, J.K., Calk, L.C., Shervais, J.W., Nielson, J.E., Schwartzman, E.C., 1988. Mafic and ultramafic xenoliths from volcanic rocks of the western United States. U.S. Geological Survey Professional Paper 1443. 179 pp.

Wilson, D., Aster, R., LA RISTRA Team, 2003. Imaging crust and upper mantle seismic structure in the southwestern United States using teleseismic receiver functions. Lead. Edge 22 (3), 232–237.